The role of catalyst–support interactions in oxygen evolution anodes based on Co(OH) 2 nanoparticles and carbon microfibers

Laura Mallón, Nuria Romero, Alicia Jiménez, Elena Martín Morales, José Alemán, Rubén Mas-Ballesté, Roger Bofill, Karine Philippot, Jordi García-Antón, Xavier Sala

ARTICLE

Received 00th January 20xx,
Accepted 00th January 20xx

DOI: 10.1039/x0xx00000x

The Role of Catalyst-Support Interactions in Oxygen Evolution Anodes based on $Co(OH)_2$ Nanoparticles and Carbon Microfibers

Laura Mallón,[a,b] Nuria Romero,[a] Alicia Jiménez,[c] Elena Martín-Morales,[a,b] José Alemán,[d] Rubén Mas-Ballesté,[c] Roger Bofill,[a] Karine Philippot,*[b] Jordi García-Antón,*[a] Xavier Sala*[a]

The performance of OER anodes based on supported nanocatalysts is highly dependent on the interactions taking place at the interface between the nanocatalyst and the employed conductive support. Herein, the versatility offered by the organometallic approach for the synthesis of metal-based nanostructures allowed preparing electrodes of tailored nanocatalyst-support interactions. A set of OER working electrodes based on $Co(OH)_2$ nanoparticles (NPs) and carbon microfibers (CFs) were prepared. The so-obtained systems differ in either the stabilizer present at the surface of the NPs (THF or 1-heptanol), the surface functionalization of the used CFs (bare CFs or oxidized-CFs) or the growth of the NPs in the presence (*in-situ*) or the absence (*ex-situ*) of the carbonaceous support. Correlation of a detailed structural and compositional analysis with the electroactivity of the tested nanomaterials allows extracting valuable insights about the influence of the metal-support interface on the OER performance of the studied anodes.

Introduction

The constant growth of the global energy demand and the consequent increase in the consumption of fossil fuels have led to the unceasing accumulation of anthropogenic CO_2 into the atmosphere and, consequently, to the global warming of our planet.[1] Thus, fighting against the consequent climate change relies on the development of new energy conversion schemes based on sustainable carbon-neutral energy sources. In this regard, the production of H_2 as energy carrier through catalytic water splitting (WS) constitutes an attractive solution when triggered by renewable sources.[2]

Common WS electrolyzers work in a division of labour approach where the two constituting half-reactions, namely the oxygen evolution reaction (OER, $2H_2O \rightarrow O_2 + 4H^+ + 4e^-$, 1.23 V_{NHE}) and the hydrogen evolution reaction (HER, $2H^+ + 2e^- \rightarrow H_2$, 0 V_{NHE}), take place in separate compartments. Both half-reactions require the use of catalysts to decrease their activation energies and increase the associated reaction rates, thus making the whole WS process viable from a practical perspective. Being the OER particularly demanding from both thermodynamic and kinetic points of view, the development of efficient, robust and easy to engineer electrodes based on earth-abundant metals for this reaction is particularly challenging. Currently, highly active but scarce noble-metal based electrocatalysts (typically IrO_x and RuO_2) are still the anodic materials of choice in commercial devices, which hampers the upgrading of the WS technology to practical large-scale applications. To face this, first-row transition metal based oxides and hydroxides have attracted enormous attention in the last decade.[3] Among them, Co-containing nanocatalysts and their corresponding composite materials arise as promising alternatives to noble-metal based OER anodes. This is due to their good balance between intrinsic activity, stability against corrosion and feasible morphology tailoring through well-stablished synthetic methodologies.[4] In this regard, we have recently reported the preparation of ligand/photoabsorber-capped Co_3O_4 nanoparticles (NPs) through the so-called organometallic approach followed by air oxidation and their successful application as catalysts for the OER.[5] However, non-supported cobalt oxide/hydroxide nanocatalysts suffer from (a) low conductivity (typically in the 10^{-2}-10^{-3} S m^{-1} range)[6] and (b) fast agglomeration under OER turnover conditions.[5,7] Therefore, the use of appropriate conductive supports is required to overcome these shortcomings.

[a] Departament de Química, Universitat Autònoma de Barcelona, Cerdanyola del Vallès, 08193 Barcelona, Spain. Email. Jordi.GarciaAnton@uab.es Xavier.Sala@uab.cat
[b] CNRS, LCC (Laboratoire de Chimie de Coordination), UPR8241, Université de Toulouse, UPS, INPT, F-31077 Toulouse cedex 4, France, Karine.Philippot@lcc-toulouse.fr
[c] Department of Inorganic Chemistry (module 07), Facultad de Ciencias, Universidad Autónoma de Madrid, Madrid, Spain
[d] Department of Organic Chemistry (módulo 01), Facultad de Ciencias, Universidad Autónoma de Madrid, Madrid, Spain
Electronic Supplementary Information (ESI) available: See DOI: 10.1039/x0xx00000x

Carbon-based materials (i.e. carbon nanotubes, graphene, etc.) have shown to be excellent supports for electrochemical applications due to their high electrical conductivity and their versatile morphology, surface chemistry, and electronic structure.[8] Additionally, the introduction of heteroatoms (i.e. N, P, S, O or B) into their structure has shown to be a powerful strategy to tune/tailor their physicochemical properties like electrical conductivity. As reported for many catalytic processes, the increase of electrical conductivity with modified carbon supports has positive effects on the activity of their corresponding supported-nanocatalysts, but also on their stability (due to limited aggregation under electrocatalytic conditions and so increased number of exposed active sites).[9,10] The use of low-dimensional carbon supports such as nanotubes or graphene entails major advantages such as high surface areas and feasible tailoring of the electronic structures through quantum confinement effects.[11] However, their engineering onto practical WS electrodes is intricate, requiring efficient deposition methods onto macroscopic electrodes (i.e. glassy carbon, FTO) which is still a challenge. In this regard, our recent report on the use of high-surface area carbon microfibers (CFs) produced by the pyrolysis of polyacrylonitrile (PAN) as either organo-electrocatalytic materials[12] or Ru NP supports[13] proved to be an efficient way to easily access working electrodes for electrocatalytic HER. CFs present a graphene-like structure containing pyridyl moieties that can be easily oxidized to generate carboxylic acid groups, producing nicotinic fragments in their structure. Bare and functionalized CFs (CF and ox-CF, respectively) can be easily handled and simply integrated in WS electrolyzers acting themselves as working electrodes (Figure 1b).

The catalytic performance and long-term stability of OER electro-anodes made of supported-nanocatalysts is highly dependent on the interactions taking place at the metal-support interface.[14,15,16] Nevertheless, thorough studies comprising the effect of systematic variations on the surface characteristics of both nanocatalysts and supports are scarce.[17] Here on, we have exploited the modularity of the organometallic approach for the synthesis of metal-based NPs in order to prepare a set of OER working electrodes based on $Co(OH)_2$ NPs and CFs for comparison purpose. The prepared electro-anodes differ in either the stabilizer present at the surface of the NPs (THF or 1-heptanol), the use of bare or functionalized CFs as a support (CF or ox-CF) or the growth of the NPs in the presence (*in-situ*) or the absence (*ex-situ*) of the carbonaceous support. Correlation of a detailed structural and compositional analysis with the observed electroactivity of the tested nanomaterials allows extracting valuable insights about the influence of the metal-support interface on the OER performance of the studied anodes.

Results and Discussion

Synthesis and Characterization of the hybrid anodes.

Six different systems (Figure 1) arising from the combination of Co-based NPs and CFs have been prepared for their study as OER anodes in alkaline media. Two types of CFs were used as supports for the NPs: as prepared CFs from poly-acrylonitrile (CF) and functionalized CFs having carboxylic groups on their surface (ox-CF), the latter resulting from oxidation of CF under a 1:1 H_2SO_4/H_2O_2 mixture (Figure 1b).[12] The graphitic regions of the CFs were not massively altered during the oxidation process, thus preserving their electrical conductivity.[12] TEM images of both supports are shown in Figure S1 in the Supplementary Information.

ARTICLE

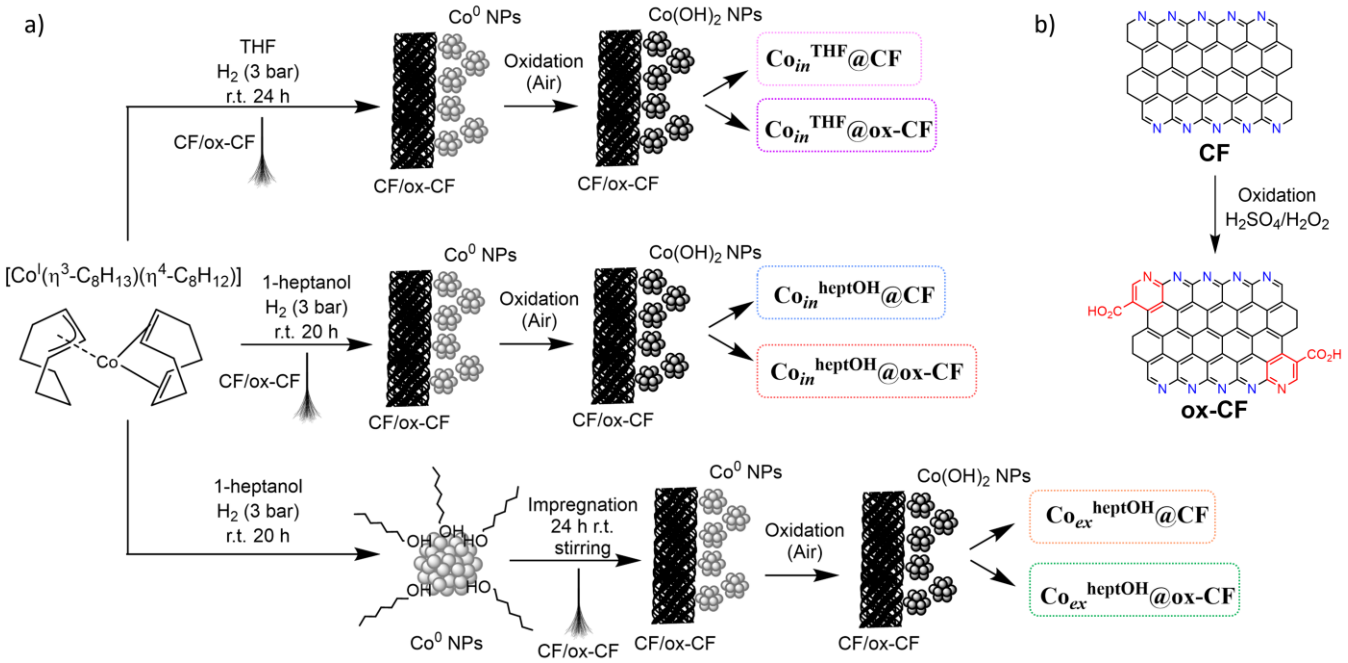

Figure 1. a) Experimental procedure for the preparation of the hybrid anodes described in this work. b) Schematic representation of the surface chemical composition of CF and ox-CF.

The incorporation of metallic Co NPs onto the CF and ox-CF supports has been performed by two different methods (*in-situ* and *ex-situ*) taking benefit of the organometallic approach for the synthesis of well-controlled metal nanostructures. The *in-situ* method consisted in the synthesis of the metallic Co NPs onto the surface of the CFs through the reductive (3 bar H_2) decomposition of the (cyclooctadienyl)(1,5-cyclooctadiene)cobalt(I), $[Co^I(\eta^3\text{-}C_8H_{13})(\eta^4\text{-}C_8H_{12})]$, complex acting as a metal precursor, in the presence of the supports either in THF or 1-heptanol at r.t. (Figure 1a, top and middle for THF and 1-heptanol, respectively). Both CF and ox-CF were simultaneously placed in the reaction vessel to ensure same reaction conditions for the two different CF-supported materials prepared in either THF or 1-heptanol, with a Co/CFs ratio of ≈ 1.2 wt.%. In this case, the internal carbon structure of CFs, the surface carboxylic groups when present (i.e. ox-CF), and the solvent (i.e. THF or 1-heptanol) can all contribute to the stabilization of the metallic Co NPs due to their direct growth onto the CFs surface. The *ex-situ* method is a two-step procedure. First, a pre-synthesis of Co NPs has been performed and the obtained colloidal suspension further used to impregnate the CFs. As THF is not able to stabilize Co NPs by itself, only 1-heptanol was used as solvent in this case. Co^{heptOH} NPs[5] (Figure S2) were thus first obtained by decomposing

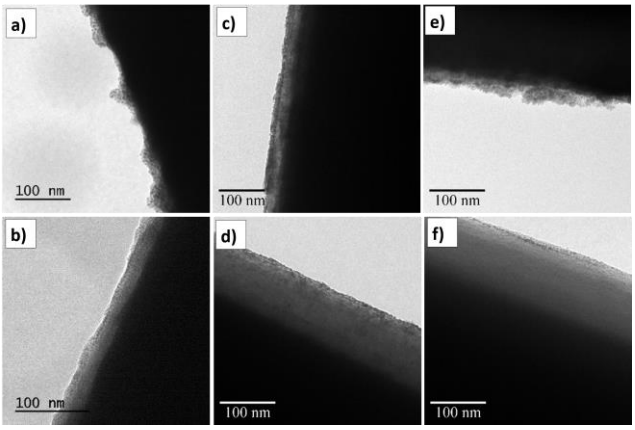

$[Co^I(\eta^3\text{-}C_8H_{13})(\eta^4\text{-}C_8H_{12})]$ in 1-heptanol at r.t. under 3 bar of H_2. Then, CFs (either CF or ox-CF) were immersed in the obtained colloidal suspension of metallic Co NPs for the impregnation step (vigorous stirring under inert conditions, 24h, r.t.) (Figure 1, bottom), leading to the attachment of the NPs onto the CFs surface. All prepared systems were then exposed to ambient air to achieve the oxidation of the metal before their test evaluation in electrocatalysis. Thus, the combination of two

synthetic methods, two types of CFs and two solvents allowed to obtain six different electrodes that will be hereafter labelled as indicated in Figure 1a.

After the oxidation step, the six materials were analysed by transmission electron microscopy (TEM). As shown in Figure 2, in all cases TEM images evidenced the presence of a thin layer of small NPs onto the CFs surface. Though some aggregates can be observed in some regions, in general the NPs are homogeneously distributed onto the CFs surface where they form a quite continuous layer. However, for the **Co_{in}^{THF}@CF** and **Co_{ex}^{heptOH}@CF** systems (Figure 2 a and e, respectively), more agglomerates together with more naked zones (i.e. without NPs) have been repeatedly observed indicating a more heterogeneous distribution of the $Co(OH)_2$ nanocatalyst in these cases. The precise mean size of the $Co(OH)_2$ NPs was difficult to measure due to their ultra-small nature (≈2 nm) and their presence at the surface of the bulky CFs (≈8 μm of diameter) which made highly challenging to get well-focused TEM images. However, it is estimated to be comprised within 1.8-2.8 nm range for all the studied systems (see Table 1).

Figure 2. Representative TEM images of the hybrid materials; a) **Co_{in}^{THF}@CF**, b) **Co_{in}^{THF}@ox-CF**, c) **Co_{in}^{heptOH}@CF**, d) **Co_{in}^{heptOH}@ox-CF**, e) **Co_{ex}^{heptOH}@CF** and f) **Co_{ex}^{heptOH}@ox-CF**.

The comparison of the four *in-situ* systems (Table 1) shows that the use of CFs with surface carboxylic groups (ox-CF systems) leads to smaller NPs than the bare support (CF systems) which can be explained by a better stabilization by the –COOH functions. In addition, the synthesis solvent (i.e. THF or 1-heptanol) does not seem to play a key role in the Co NP stabilization during the synthetic process, as comparable NPs sizes and morphologies are observed between analogous *in-situ* systems (**Co_{in}^{THF}@CF/Co_{in}^{heptOH}@CF** and **Co_{in}^{THF}@ox-CF/ Co_{in}^{heptOH}@ox-CF**).

XPS analysis was performed on the six prepared nanomaterials in order to determine the nature of the cobalt species present in each electrode (Figure S3). The main peaks observed can be clearly indexed to O 1s, N 1s, C 1s and Co 2p regions. Focusing on the Co 2p region, the high-resolution XPS spectra of the whole set of materials are shown in Figure S4 and a summary of the most relevant data is presented in Table S1. Given the high similarity of all the obtained spectra, only that of **Co_{in}^{heptOH}@CF** is reported in Figure 3 as a representative example. Two main peaks at a binding energy (BE) of ≈781-782 eV and ≈796-797.5 eV corresponding to the $2p_{3/2}$ and $2p_{1/2}$ levels, respectively, are observed in all cases. Besides the normal core photoelectron lines, strong satellite peaks at ca. 3.9-7.4 eV higher energy than the main peaks are also observed. These additional spectral lines can be related either to a coupling between unpaired electrons in the atom (multiplet splitting) or a multiple electron excitation (shake-up). It is well-known that high spin cobalt(II) compounds have intense satellite bands, while satellite lines for the low spin cobalt(III) compounds are either weak or missing.[18,19] The peaks observed in the Co region 2p thus indicate the presence of high spin cobalt(II) species in the six prepared materials. Moreover, the O1s spectra shown in Figure S5, show strong peaks at relatively high BE (531-533 eV) for all samples. According to literature data,[19,20] where O from hydroxides appears on the higher BE side of the spectrum (531-533 eV) whereas O from oxides appears at lower BE (529-530 eV), our results indicate the presence of -OH moieties bonded to Co(II). Taken all together, XPS data evidence the presence of supported $Co(OH)_2$ NPs in all prepared systems. The low oxidation state of Co here found for **Co_{ex}^{heptOH}@CF** and **Co_{ex}^{heptOH}@ox-CF** contrasts with that recently reported for the corresponding non-supported Co NPs prepared under similar reaction conditions, where a mixed $Co^{II}Co^{III}{}_2O_4$ (Co_3O_4) species was detected.[5] This fact highlights the reductive nature of the carbonaceous support here employed and its decisive role in the final oxidation state of the Co nanocatalysts when oxidized from metallic Co on its surface in the applied oxidation conditions.

Figure 3. High-resolution XPS analysis in the Co 2p region for **Co_{in}^{heptOH}@CF** (black). Deconvolution of Co peaks (blue line) and envelope (red).

ICP-OES analyses (see Table 1) revealed Co contents ≤ 0.23 wt.% for all samples. A quick glance at these data in Table 1 reveals that *in-situ* systems (entries 1-4) incorporate higher Co loadings than their *ex-situ* counterparts (entries 5-6). This observation points to the detrimental effect of the *ex-situ* method where 1-heptanol acts as Co NPs stabilizer and can limit the deposition of the Co NPs during the impregnation step due to either steric effects between its carbon chains or weak interaction of the latter with the carbon structure of the CFs.

Electrocatalytic performance in the OER.

The six electrodes prepared in this work arise from the combination of two CF supports of different surface composition and $Co(OH)_2$ NPs prepared by means of two different methods *(in-situ* or *ex-situ)* where the *ex-situ* method required the use of a stabilizer (1-heptanol), and thus constitute an ideal platform to systematically study the role of catalyst-support interactions in OER anodes. In order to evaluate their electrocatalytic performance, 1-mg working electrodes were prepared (see the Experimental Section for further details) and immersed in a 0.1 M NaOH aqueous solution at pH 13. As shown in Figure 4a-b, when scanned anodically up to 1.25 V *vs.* NHE all electrodes showed two anodic peaks in the oxidative forward scan prior to

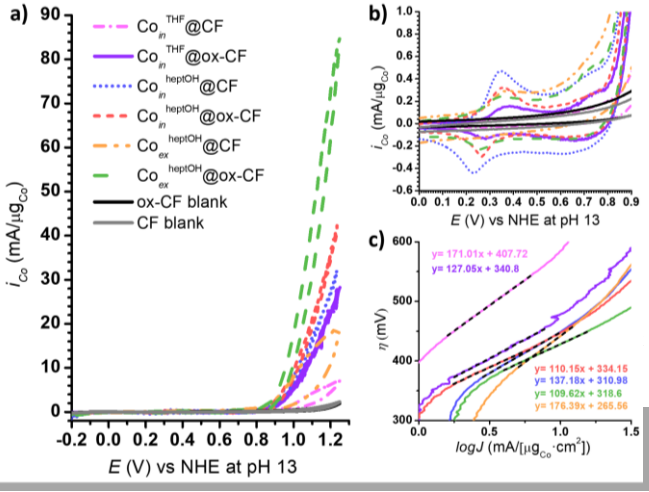

a sharp current increase assigned to the electrocatalytic oxidation of water to dioxygen. According to literature data,[21,22] the first faradaic process observed in the voltammogram (E_{ap}=0.36 V vs NHE) could be attributed to the oxidation of Co(II) to Co(III) and the second one, appearing at a higher anodic potential (E_{ap}=0.76 V vs NHE) and partially masked with the electrocatalytic current, to the subsequent oxidation of Co(III) to Co(IV). Interestingly, the Co(IV) is usually proposed as the active species towards the OER in related Co-based systems.[23,24,25] The two cathodic waves in the backward scan correspond to the complementary reduction processes.

Figure 4. a) Cyclic Voltammograms (CVs) in a 0.1 M NaOH aqueous solution at pH 13 of a) **Co_{in}^{THF}@CF** (pink), **Co_{in}-^{THF}@ox-CF** (purple), **Co_{in}^{heptOH}@CF** (blue), **Co_{in}^{heptOH}@ox-CF** (red), **Co_{ex}^{heptOH}@CF** (orange) and **Co_{ex}^{heptOH}@ox-CF** (green). ox-CF (black) and CF (grey) blanks are also shown. b) Zoom in the potential range at which the Co(III/II) and Co(IV/III) redox events occur. c) Tafel plots of all materials studied in this work (colour code as in a).

In order to benchmark the catalytic activity of the six studied electrodes, the intensity of the OER electrocatalytic current observed in the cyclic voltammograms (CV) displayed in Figure 4a has been normalized by the Co wt.% in each case and labelled as i_{Co} = [mA/μg_{Co}], thus allowing a fair comparison of the electroactivity between samples holding different Co loadings. Furthermore, stability studies were carried out by the CV monitoring of i_{Co} after different times of exposure of the samples to chronoamperometric conditions (1 V vs. NHE at pH 13, Figures S6-S8 and Table S2). A summary of the most relevant figures of merit defining the electrocatalytic activity and short-term stability of the studied anodes in the OER can be found in Table 1.

Table 1. Physico-chemical and OER electrocatalytic data for the anodes studied in this work (0.1 M NaOH aqueous solution at pH 13).

Entry	System	Ø (nm)	Co (wt.%)	η_0[(a)] (mV)	Tafel slope (mV · dec^{-1})	$i_{Co\ t=0\ s}$ (mA/μg_{Co})	$i_{Co\ t=10\ min}$ (mA/μg_{Co})	$i_{Co\ t=2h}$[(b)] (mA/μg_{Co})	$i_{Co\ REM}$[(c)] (%)
1	**Co_{in}^{THF}@CF**	2.6 ± 0.7	0.13	342	171	7.2	28.2	8.9	32
2	**Co_{in}^{THF}@ox-CF**	1.8 ± 0.4	0.23	327	127	28.3	20.1	14.1	50
3	**Co_{in}^{heptOH}@CF**	2.8 ± 0.6	0.14	307	137	32.9	39.3	25	64
4	**Co_{in}^{heptOH}@ox-CF**	2.1 ± 0.4	0.13	307	110	42.3	34.6	26.2	62
5	**Co_{ex}^{heptOH}@CF**	2.0 ± 0.5	0.039	322	176	19.2	46.2	25.6	55
6	**Co_{ex}^{heptOH}@ox-CF**	2.3 ± 0.5	0.055	312	110	85.5	56.1	37	43

a) η_0 is calculated as $\eta_0 = E_{Hg/Hg2SO4,\ K2SO4(sat'd)} + 0.65\ V - (1.23 - 0.059 \cdot 13)$, where $(1.23 - 0.059 \cdot 13)$ is the theoretical thermodynamic potential at which water is oxidized at pH 13 and $E_{Hg/Hg2SO4,\ K2SO4(sat'd)}$ is the experimental potential at which an abrupt increase of the current intensity starts in the CV.
b) i_{Co} t=2h measured after removing all the bubbles formed on the system and performing IR drop correction at 85% again.
c) % $i_{Co\ REM}$ calculated by dividing $i_{Co\ t=2\ h}$ by $i_{Co\ t=0\ s}$ as short-term stability data for ox-CF systems and by dividing $i_{Co\ t=2\ h}$ by $i_{Co\ t=10\ min}$ (value after activation) as short-term stability data for CF systems.

The recorded onset overpotentials (η_0, 307-342 mV range) and Tafel slopes (110-176 mV·dec^{-1}) are comparable to those reported for related carbon-supported Co-based OER electrocatalysts under alkaline conditions (see Table S3). However, a close look at the other data in Table 1 allows extracting valuable information about the effect that the different catalyst-support interfaces have on the resulting OER performance of the set of studied anodes.

The presence of carboxylic acid groups at the surface of the CFs (i.e. ox-CF) has a remarkable positive effect in the electrocatalytic performance of the studied systems, promoting increased normalized current intensities, lower Tafel slopes and slightly lower onset overpotentials (see Table 1). Even if this trend is general for all the CF/ox-CF pairs studied, CF surface oxidation has maximum benefits in THF stabilized (entries 1 and 2) and *ex-situ* (entries 5 and 6) systems, where normalized current intensities increase by a factor of 4 and Tafel slopes (Figure 4c and Table 1) decrease nearly 35% in both cases. The positive effect of surface functionalization in ox-CF electrodes could arise from coordinative or/and H-bond interaction between surface carboxylate groups of the support and the $Co(OH)_2$ NPs, improving the electronic communication between catalyst and support and easing the attainment of high oxidation states through the anionic nature of the -COO^- scaffolds. The tendency to obtain slightly smaller NPs when ox-CF electrodes are used (entries 1 and 2 and entries 3 and 4 in Table 1) also supports the stabilizing role of surface carboxylates and thus their interaction with the Co-based species. The higher surface/volume ratio and thus higher number of active sites present in the smaller in size $Co(OH)_2$ NPs present in ox-CF-based systems can also contribute to the observed enhanced OER activity with these electrodes. Also, as recently described for molecular complexes,[26] the potential role of dangling

carboxylates from the ox-CF support as proton acceptor moieties (internal bases) lowering the activation free energies that lead to O-O bond formation in the OER cannot be discarded. Additionally, the absence of stabilizing groups at the surface of bare CF electrodes led to $Co(OH)_2$ NPs less dispersed on the support (see above), which probably reduces the number of exposed active sites and contributes to further decrease of the observed i_{Co} values with these electrodes. In contrast, the less amount of Co in *ex-situ* materials could help to obtain a thinner and more homogeneous film of $Co(OH)_2$ NPs, thus obtaining a material with higher exposed active sites. This fact could also leads to a better interaction between the $Co(OH)_2$ nanoparticulated catalyst and the support C surface, obtaining higher catalytic activities per µg of Co (i.e. higher intensities).

The evolution of the normalized electrocatalytic current intensities (i_{Co}) measured by CV after certain time (0, 10, 30, 60 and 120 min.) under chronoamperometric OER conditions (1 V vs NHE in 0.1 M NaOH) reveals again a distinct behaviour between CF and ox-CF electrodes. As can be observed in Figures S6-S8 and Table 1 and S2, while the i_{Co} of ox-CF electrodes progressively decreases with time ($i_{Co\ t=0} > i_{Co\ t>0}$) in all cases (entries 2, 4 and 6 in Table 1) due to deactivation pathways (see below for more details), CF anodes firstly activate ($i_{Co\ t=0} < i_{Co\ t=10'}$, entries 1, 3 and 5) prior to progressively deactivate after longer time under turnover conditions. For this reason, a complementary comparison of CV profiles and corresponding Tafel plots of ox-CFs at t= 0 s and CFs at t=10 min (after activation) is shown in Figure S9. Again, this behaviour could be explained by the different catalyst-support interactions present in each case. Therefore, the electronic communication between the bare CF electrodes and $Co(OH)_2$ NPs seems initially weak and its improvement (and concomitant activation) under OER conditions could be related to the partial removal of stabilizer. Contrarily, the electronic communication (through coordinative COO-$Co(OH)_2$ bonds or/and H-bonds) seems optimum in ox-CF anodes, where no activation is observed.

Irrespective of the presence or not of activation process, the i_{Co} values progressively decrease in all systems and only part of the initial electrocatalytic current is maintained after 2h under chronoamperometric OER conditions ($i_{Co\ REM}$ in Table 1 and Figure S8). Provided the same stabilizer (1-heptanol) is used and irrespective of the CF/ox-CF nature of the support, when $i_{Co\ REM}$ is compared for *in-situ* and *ex-situ* systems the former tends to be slightly more robust than the latter. This observation highlights the stronger catalyst-support interaction attained when the NPs are directly grown onto the supports. Among *in-situ* electrodes, the surface functionalization of the support (ox-CF) is only beneficial when THF, a weak stabilizer, is used as solvent for the electrode preparation process (compare $i_{Co\ REM}$ in THF entries 1 and 2 vs. $i_{Co\ REM}$ in entries 3 and 4 where 1-heptanol is used). Therefore, when the support becomes the main stabilizing agent for $Co(OH)_2$ NPs the role of surface carboxylic acid groups in ox-CF is clearly emphasized. Contrarily, when the stability of the two *ex-situ* anodes is compared ($i_{Co\ REM}$ in entries 5 and 6) the presence of carboxylic acid groups in the support (ox-CF) is not beneficial but even detrimental. Therefore, the presence of surface carboxylate groups in ox-CF seems to destabilize the resulting electrodes, potentially through steric interactions of the carboxylate moieties with the 1-heptanol that stabilizes the preformed NPs.

In order to shed some light on the observed deactivation pathways occurring in the prepared anodes under OER conditions, a set of complementary analyses were carried out. Thus, after a 2 h chronoamperometric experiment (1 V *vs* NHE, 0.1 M NaOH) TEM images of the full set of working electrodes were recorded. Images after catalysis revealed a more heterogeneous distribution of the Co NPs onto the surface of the CFs, showing regions with big aggregates together with naked areas in the supports (Figure S10). Together with their aggregation under turnover conditions that decreases the number of exposed active sites, the mechanical leaching of the NPs, and/or the evolution of $Co(OH)_2$ to other phases with reduced OER activity could also be at the origin of the observed decrease in activity over time. Thus, selecting **Co_{in}^{heptOH}@ox-CF** as representative anode, XPS and ICP-OES analyses were carried out after 2 h under electrocatalytic conditions. XPS analysis revealed comparable Co 2p and O 1s binding energies before and after catalysis (Figure S11 and Table S1), thus confirming $Co(OH)_2$ as the Co species present at the electrode surface after catalytic turnover. Additionally, ICP data revealed both a clear decrease in the Co content at the electrode surface (from 0.13 wt.% to 0.05 wt.%), and the presence of Co in the resulting 0.1 M NaOH solution (0.4 mg/L). Thus, both the aggregation and partial leaching of the $Co(OH)_2$ NPs under OER electrocatalytic conditions seem to be at the origin of the observed deactivation. Finally, the Faradaic efficiency (Ɛ, %) of all hybrid anodes was evaluated by a 20-minute O_2-monitored chronoamperometry at a fixed potential of 1 V vs NHE at pH 13. As shown in Figure S12, Ɛ > 90% was observed in all cases. Thus, even if partial deactivation due to aggregation and leaching takes place under the applied OER conditions, the high Faradaic efficiency confirms oxygen evolution as the sole reaction happening in the studied anodes.

Conclusions

This contribution highlights the suitability of the organometallic approach for the synthesis of nanostructures to systematically tailor the interface between nanocatalysts and carbon-based supports in OER electro-anodes. Hence, the use of bare (CF) and surface-functionalized (ox-CF) carbon microfibers as cheap, easy to engineer, high-surface area supports combined with the versatility of the synthetic method (permitting the use of different NP stabilizers and their synthesis in the presence -*in-situ*- or absence -*ex-situ*- of the carbonaceous support) allowed obtaining a set of six $Co(OH)_2$@CF/ox-CF electrodes of different interfacial nature.

The morphological (TEM) and compositional (XPS, ICP, EDX) characterization of the series of prepared electrodes together with their evaluation as OER electrocatalysts under alkaline conditions allowed extracting several substantial conclusions about the role that catalyst-support interactions have in the

observed electrocatalytic performance. First, the presence of carboxylic groups at the surface of the CFs support (ox-CF electrodes) has shown to play a major role on both the morphology (systematically reducing the NPs size and increasing their dispersion at the electrode surface) and the OER performance (increasing the activity and stability in the OER, particularly when the weak stabilizer THF is employed) of the prepared electrodes. These observations point to the likely formation of COO-$Co(OH)_2$ coordinative bonds or/and H-bonds improving both the electronic communication between catalyst and support and the dispersibility and stability of the former on top of the latter. Second, systems prepared *in-situ* displayed higher Co loadings and higher stabilities under electrocatalytic OER conditions than their corresponding counterparts prepared *ex-situ* by an impregnation step, thus evidencing the formation of stronger catalyst-support interactions when the nanocatalysts are directly grown at the surface of the CFs.

Finally, the studied anodes maintain $Co(OH)_2$ as catalytic species after 2 h of electrocatalytic turnover. Even if they partially deactivated due to both aggregation and leaching of the NPs from the electrode surface, almost quantitative Faradaic efficiencies show oxygen evolution as the only redox reaction occurring at their surface.

All in all, the results reported here on evidence how subtle surface modifications of either the catalyst or the support in OER anodes can lead to significantly different catalytic outputs, and thus highlight the need of more systematic research focused to explore the nature of catalyst-support interfaces.

Experimental

Materials and methods

All procedures concerning the synthesis and preparation of samples were carried out using standard Schlenk tubes, Fisher-Porter glassware and vacuum line techniques or in a glove-box (MBraun) under argon atmosphere. Solvents (THF, pentane) were purified before use by filtration on adequate alumina columns in a purification apparatus (MBraun) and handled under argon atmosphere. Reagents and solvents were degassed before use via a multi-cycle freeze-pump-thaw process. The (cyclooctadienyl)(1,5-cyclooctadiene)cobalt(I) complex, $[Co^{I}(\eta^3\text{-}C_8H_{13})(\eta^4\text{-}C_8H_{12})]$, was purchased from Nanomeps-Toulouse. Dihydrogen and argon were purchased from Alphagaz. 1-Heptanol was acquired from Sigma-Aldrich and dried over activated molecular sieves (4Å) prior to use. Other reagents were employed as received unless otherwise specified. Carbon fibers (CFs) (Twill 2x2 3K weight 200 g/m^2 width 1200 mm, Model HA2301) were purchased from ClipCarbono.

Synthetic procedures

CFs Electrode Preparation. CFs electrodes have been prepared as stated in reference 12. Commercial CFs consist of bundles of around 3000 filaments of 5-8 μm of diameter. The CFs electrodes contain 7 bundles of 3000 filaments (21000 filaments) making a 6 cm long brunch of fibers. Then, this 6 cm long brunch was folded in half, obtaining electrodes (≈90 mg) containing the double of filaments (42000) but only with 2 cm exposed for NPs synthesis and electrode usage. The ready-made electrodes (CF) are treated with commercial sulfuric acid (98%) at room temperature with stirring and later introduced into a 1:1 H_2SO_4/H_2O_2 mixture for 1 h to obtain the oxidized CFs (ox-CF). After the synthesis of the NPs onto the CFs electrodes and before the catalytic evaluation, these brushes were cut in 3-cm-long filaments (half fiber). 1 mg of these filaments was attached to a Cu tape together with a Cu-wire and everything was tight with a Teflon tape, still ensuring 2 cm length for the catalytic experiments.

Synthesis of Co_{in}^{THF}@CF and Co_{in}^{THF}@ox-CF. Under argon atmosphere, one brush of each type of CFs (~90 mg) was introduced into a Fisher-Porter reactor containing 10 mL of THF and $[Co^{I}(\eta^3\text{-}C_8H_{13})(\eta^4\text{-}C_8H_{12})]$ (10 mg, 0.036 mmol), leading the two ends of each brush to be soaked in the reaction media. The Fischer-Porter was then pressurized with 3 bar of dihydrogen and the reaction mixture kept at r. t. under vigorous stirring for 24 h. After the reaction time, the remaining H_2 was removed under vacuum. The obtained materials were washed by soaking them in degassed anhydrous pentane (x3) and dried under vacuum. Both CFs brushes were exposed to air to achieve the oxidation of the as-synthesized metallic Co NPs. **Co_{in}^{THF}@CF**: TEM: Ø = 2.6 ± 0.7 nm, ICP(Co wt.%): 0.13%, XPS: $Co(OH)_2$ $2p_{3/2}$ (781.4 eV) satellites (785.4 eV) $2p_{1/2}$ (797.3 eV) satellites (800.8 eV). **Co_{in}^{THF}@ox-CF**: TEM: Ø =1.8 ± 0.4 nm, ICP-OES (Co wt.%): 0.23%, XPS: $Co(OH)_2$ $2p_{3/2}$ (781.5 eV) satellites (785.4 eV) $2p_{1/2}$ (797.3 eV) satellites (802.9 eV)

Synthesis of Co_{in}^{heptOH}@CF and Co_{in}^{heptOH}@ox-CF. Under argon atmosphere, one brush of each type of CFs (~90 mg) was introduced into a Fisher-Porter reactor containing 10 mL of 1-heptanol and $[Co^{I}(\eta^3\text{-}C_8H_{13})(\eta^4\text{-}C_8H_{12})]$ (10 mg, 0.036 mmol), leading the two ends of each brush to be soaked in the reaction media. The Fischer-Porter was then pressurized with 3 bar of dihydrogen and the reaction mixture kept at r. t. under vigorous stirring for 20 h. After the reaction time, the remaining H_2 was removed under vacuum. The obtained materials were washed by soaking them in degassed anhydrous pentane (x3) and dried under vacuum. Both CFs brushes were exposed to air to achieve the oxidation of the as-synthesized metallic Co NPs. **Co_{in}^{heptOH}@CF**: TEM: Ø = 2.8 ± 0.6 nm, ICP-OES (Co wt.%): 0.14%, XPS: $Co(OH)_2$ $2p_{3/2}$ (781.7 eV) satellites (785.6 eV) $2p_{1/2}$ (797.4 eV) satellites (803.0 eV). **Co_{in}^{heptOH}@ox-CF**: TEM: Ø =2.1 ± 0.4 nm, ICP-OES (Co wt.%): 0.13%, XPS: $Co(OH)_2$ $2p_{3/2}$ (781.6 eV) satellites (786.9 eV) $2p_{1/2}$ (796.9 eV) satellites (804.3 eV)

Synthesis of Co_{ex}^{heptOH}@CF and Co_{ex}^{heptOH}@ox-CF. Under Ar atmosphere, $[Co^{I}(\eta^3\text{-}C_8H_{13})(\eta^4\text{-}C_8H_{12})]$ (10 mg, 0.036 mmol) was introduced into a Fischer-Porter reactor. Next, anhydrous 1-heptanol (10 mL) was transferred to the reactor vessel *via cannulae*. The Fischer-Porter was then pressurized with dihydrogen (3 bar) and the reaction mixture kept at r. t. under vigorous stirring for 20 h. After the reaction time, the remaining H_2 was removed under vacuum and one brush (~90 mg) of each type of CFs (CF/ox-CF) were introduced into the reactor leading the two ends of each brush soaked in the reaction media. They

were let impregnating for 24 h under Ar atmosphere, at r. t. and under vigorous stirring. Finally, both brushes were washed by soaking them in degassed anhydrous pentane (x3) and dried under vacuum. Both CFs brushes were finally exposed to air to achieve the oxidation of the as-synthesized metallic Co NPs. **Co_{ex}^{heptOH}@CF**: TEM: Ø = 2.0 ± 0.5 nm, ICP-OES (Co wt.%): 0.039%, XPS: $Co(OH)_2$ $2p_{3/2}$ (781.2 eV) satellites (785.9 eV) $2p_{1/2}$ (797.4 eV) satellites (804.2 eV). **Co_{ex}^{heptOH}@ox-CF**: TEM: Ø =2.3 ± 0.5 nm, ICP-OES (Co wt.%): 0.055%, XPS: $Co(OH)_2$ $2p_{3/2}$ (781.0 eV) satellites (785.5 eV) $2p_{1/2}$ (797.1 eV) satellites (803.1 eV).

Characterization Techniques

Transmission electron microscopy (TEM). Observations for the colloidal system were performed at the "UMS 3623 – Centre de microcaractérisation Raimond Castaing" using a MET JEOL JEM 1011 electron microscope operating at 100 kV with resolution point of 4.5 Å. TEM grids were prepared by drop-casting of the crude 1-heptanol NPs colloidal solution into a carbon-coated copper grid. Pumping with a Gatan turbo pumping station model 655 was carried out before TEM analysis. Supported systems were analysed at the "Servei de Microscòpia" of the UAB using a JEOL JEM 1400 electron microscope working at 120 kV with a resolution point of 0.4 nm by depositing a small amount of CFs onto a carbon-coated copper grid just before TEM analysis. Size distributions were determined through manual analysis of enlarged micrographs with *ImageJ* software to obtain statistical size distribution and a mean diameter. For each system, the mean size was calculated by assuming a spherical shape. In all size distributions more than 200 particles were counted. Size distributions are quoted as the mean diameter ± the standard deviation (σ).

X-ray Photoelectron Spectroscopy (XPS). Measurements were performed at the Catalan Institute of Nanoscience and Nanotechnology (ICN2) using a Phoibos 150 analyzer (SPECS GmbH, Berlin, Germany) at room temperature in ultra-high vacuum conditions (base pressure $5 \cdot 10^{-10}$ mbar) with a monochromatic aluminium Kα x-ray source (1486.74 eV) as the excitation X-ray source. The energy resolution was measured by the Full Width at Half Maximum (FWHM) of the Ag $3d_{5/2}$ peak for a sputtered silver foil, which was 0.62 eV, and all data were corrected using the C1s peak at 284.8 eV as an internal standard.

Inductively Coupled Plasma Optic Emission Spectroscopy (ICP-OES). Analysis were performed at the "Servei d'Anàlisi Química" (SAQ) at the UAB, on a Perkin Elmer Optima 4300 DV system. Solid samples were treated by weighing 1 mg in an analytic balance XPE205DR (Mettler Toledo) and digesting them in a Milestone UltraWave in a mixture of concentrated HNO_3 and HCl (Merck) prior to the analysis (two replicates were performed for each sample). For liquid samples, 1 mL was digested following the same procedure as for solid samples.

Electrochemical measurements. Electrocatalytic OER experiments were performed in a 10 mL two-compartment cell with a proton exchange membrane between them at room temperature in a three-electrode configuration using Hg/Hg_2SO_4, K_2SO_4(sat'd) and Pt as reference and counter electrodes, respectively. Working electrodes (WE) were hand-made prepared using a short copper wire, 1-mg CFs brush and some Teflon tape to tight everything together. Both compartments were filled with 6 mL of 0.1 M NaOH aqueous solution and equipped with a stirring bar, being the CE placed in one compartment and the WE and RE in the other one. The potential was controlled using a BioLogic SP-150 potentiostat using the EC-Lab software for data acquisition and handling. IR drop was automatically corrected at 85% for cyclic voltammetry and chronoamperometry measurements. All catalytic experiments were recorded with a sweep rate of 100 mV/s. Potentials are reported *vs.* NHE (by adding +0.65 V) and overpotentials are calculated as

A Clark type electrode (Unisense OX-NP needle microsensor) was used to measure the produced oxygen in the gas phase during the chronoamperometry experiments by placing it together with the WE and RE in the same compartment. Faradaic Efficiencies were calculated for each system. The instrument was kept polarizing at -800 mV overnight before use. The sensor was calibrated by adding different known volumes of 99% pure oxygen at the end of the experiment.

Cyclic Voltammetry (CV). The system was scanned from E_i=-0.25 V to E_f=1.25 V *vs.* NHE at 100 mV/s.

Chronoamperometry (CA). Controlled potential chronoamperometric experiments were performed at E_{app}= 1 V *vs.* NHE.

Conflicts of interest

There are no conflicts to declare.

Acknowledgements

This work was financially supported by the MINECO/FEDER project CTQ2015-64261-R, the CNRS, the Univ. Toulouse III - Paul Sabatier and the GDRI HC3A Franco-Catalan action. L. M. thanks the UAB for a PhD grant. J.G.-A. acknowledges the Serra Húnter Program. The authors acknowledge Guillaume Sauthier for XPS analysis. We are grateful to the Spanish Government (RTI2018-095038-B-I00), "Comunidad de Madrid" and European Structural Funds (S2018/NMT-4367).

References

1. Intergovernmental Panel on Climate Change. *Global Warming of 1.5 °C* (IPCC, 2018).
2. M. A. Rosen, S. Koohi-Fayegh, *Energ. Ecol. Environ*. 2016, **1**, 10-29.
3. I. Roger, M. A. Shipman, M. D. Symes, *Nat. Rev. Chem.* 2017, **1**, 0003.
4. S. Li, X. Hao, A. Abudula, G. Guan, *J. Mater. Chem. A* 2019, **7**, 18674-18797.
5. J. De Tovar, N. Romero, S. A. Denisov, R. Bofill, C. Gimbert-Suriñach, D. Ciuculescu-Pradines, S. Drouet, A. Llobet, P.

Lecante, V. Colliere, Z. Freixa, N. McClenaghan, C. Amiens, J. García-Antón, K. Philippot, X. Sala, *Mater. Today Energy* 2018, **9**, 506-515.
6. K. M. Shaju, L. Guerlou-Demourgues, G. Godillot, W. Weill, C. Delmas, *J. Electrochem. Soc.* 2012, **159**, A1934-A1940.
7. M. S. Burke, L. J. Enman, A. S. Batchellor, S. Zhou, S. W. Boettcher, *Chem. Mater.* 2015, **27**, 7549- 7558.
8. J. Zhang, Z. Xia, L. Dai, *Sci. Adv.* 2015, **1**, e1500564.
9. A. Bähr, G.-H. Moon, H. Tüysüz, *ACS Appl. Energy Mater.* 2019, **2**, 6672-6680.
10. J. Creus, J. De Tovar, N. Romero, J. García-Antón, K. Philippot, R. Bofill, X. Sala, *ChemSusChem* 2019, **12**, 2593-2514.
11. X. Kong, Z. Peng, *Mater. Today Chem.* 2019, **11**, 119-132.
12. O. G. Moral, A. Call, F. Franco, A. Moya, J. A. Nieto-Rodríguez, M. Frias, J. L. G. Fierro, M. Costas, J. Lloret-Fillol, J. Alemán, R. Mas-Ballesté, *Chem. Eur. J.* 2018, **24**, 3305–3313
13. J. Creus, L. Mallón, N. Romero, R. Bofill, A. Moya, J. L. G. Fierro, R. Mas-Ballesté, X. Sala, K. Philippot, J. García-Antón, *Eur. J. Inorg. Chem.* 2019, 2071–2077.
14. H. Li, C. Chen, D. Yan, Y. Wang, R. Chen, Y. Zou, S. Wang, *J. Mater. Chem. A.* 2019, **7**, 23432-23450.
15. H.-S Oh, H.N. Nong, T. Reier, A. Bergmann, M. Gliech, J. Gerreira de Araújo, E. Willinger, R. Schlogl, D. Teschner, P. Strasser, *J. Am. Chem. Soc.* 2016, **138**, 12552-12563.
16. H. He, J. Chen, D. Zhang, F. Li, X. Chen, Y. Chen, L. Bian, Q. Wang, P. Duan, Z. Wen, X. Lv, *ACS Catal.* 2018, **8**, 6617-6626.
17. T. W. Van Deelen, C. Hernández-Mejia, K. P. De Jong, *Nat. Catal.* 2019, **2**, 955-970.
18. M. C. Biesinger, B. P. Payne, A. P. Grosvenor, L. W. M. Lau, A. R. Gerson, R. St. C. Smart, *Appl. Surf. Sci.* 2011, **257**, 2717-2730.
19. J. Yang, H. Liu, W. N. Martens, R. L. Frost, *J. Phys. Chem*. 2010, **114**, 111-119.
20. J. Stoch, J. Gablankowska-Kukucz, *Surf. Interface Anal*. 1991 **17**, 165-167.
21. Y. C. Liu, J. A. Koza, J. A. Switzer, *Electrochim. Acta* 2014, **140**, 359-365.
22. Y. Q. Gao, H. B. Li, G. W. Yang, J. Appl. Phys. 2016, **119**, 034902.
23. N. H. Chou, P. N. Ross, A. T. Bell, T. D. Tilley, *ChemSusChem* 2011, **4**, 1566-1569.
24. B. S. Yeo, A. T. Bell, J. Am. Chem. Soc. 2011, 133, 5587-5593.
25. M. E. G. Lyons, M. P. Brandon, *J. of Electroanal. Chem.* 2010, **641**, 119-130
26. R. Matheu, M. Z. Ertem, J. Benet-Buchholz, E. Coronado, V. S. Batista, X. Sala, A. Llobet, *J. Am. Chem. Soc.* 2015, **137**, 10786-10795.

1 Intergovernmental Panel on Climate Change. *Global Warming of 1.5 °C* (IPCC, 2018).
2 M. A. Rosen, S. Koohi-Fayegh, *Energ. Ecol. Environ*. 2016, **1**, 10-29.
3 I. Roger, M. A. Shipman, M. D. Symes, *Nat. Rev. Chem.* 2017, **1**, 0003.
4 S. Li, X. Hao, A. Abudula, G. Guan, *J. Mater. Chem. A* 2019, **7**, 18674-18797.
5 J. De Tovar, N. Romero, S. A. Denisov, R. Bofill, C. Gimbert-Suriñach, D. Ciuculescu-Pradines, S. Drouet, A. Llobet, P. Lecante, V. Colliere, Z. Freixa, N. McClenaghan, C. Amiens, J. García-Antón, K. Philippot, X. Sala, *Mater. Today Energy* 2018, **9**, 506-515.
6 K. M. Shaju, L. Guerlou-Demourgues, G. Godillot, W. Weill, C. Delmas, *J. Electrochem. Soc.* 2012, **159**, A1934-A1940.
7 M. S. Burke, L. J. Enman, A. S. Batchellor, S. Zhou, S. W. Boettcher, *Chem. Mater.* 2015, **27**, 7549- 7558.
8 J. Zhang, Z. Xia, L. Dai, *Sci. Adv.* 2015, **1**, e1500564.
9 A. Bähr, G.-H. Moon, H. Tüysüz, *ACS Appl. Energy Mater.* 2019, **2**, 6672-6680.
10 J. Creus, J. De Tovar, N. Romero, J. García-Antón, K. Philippot, R. Bofill, X. Sala, *ChemSusChem* 2019, **12**, 2593-2514.
11 X. Kong, Z. Peng, *Mater. Today Chem.* 2019, **11**, 119-132.
12 O. G. Moral, A. Call, F. Franco, A. Moya, J. A. Nieto-Rodríguez, M. Frias, J. L. G. Fierro, M. Costas, J. Lloret-Fillol, J. Alemán, R. Mas-Ballesté, *Chem. Eur. J.* 2018, **24**, 3305–3313
13 J. Creus, L. Mallón, N. Romero, R. Bofill, A. Moya, J. L. G. Fierro, R. Mas-Ballesté, X. Sala, K. Philippot, J. García-Antón, *Eur. J. Inorg. Chem.* 2019, 2071–2077.
14 H. Li, C. Chen, D. Yan, Y. Wang, R. Chen, Y. Zou, S. Wang, *J. Mater. Chem. A.* 2019, **7**, 23432-23450.
15 H.-S Oh, H.N. Nong, T. Reier, A. Bergmann, M. Gliech, J. Gerreira de Araújo, E. Willinger, R. Schlogl, D. Teschner, P. Strasser, *J. Am. Chem. Soc.* 2016, **138**, 12552-12563.
16 H. He, J. Chen, D. Zhang, F. Li, X. Chen, Y. Chen, L. Bian, Q. Wang, P. Duan, Z. Wen, X. Lv, *ACS Catal.* 2018, **8**, 6617-6626.
17 T. W. Van Deelen, C. Hernández-Mejia, K. P. De Jong, *Nat. Catal.* 2019, **2**, 955-970.
18 M. C. Biesinger, B. P. Payne, A. P. Grosvenor, L. W. M. Lau, A. R. Gerson, R. St. C. Smart, *Appl. Surf. Sci.* 2011, **257**, 2717-2730.
19 J. Yang, H. Liu, W. N. Martens, R. L. Frost, *J. Phys. Chem*. 2010, **114**, 111-119.
20 J. Stoch, J. Gablankowska-Kukucz, *Surf. Interface Anal*. 1991, **17**, 165-167.
21 Y. C. Liu, J. A. Koza, J. A. Switzer, *Electrochim. Acta* 2014, **140**, 359-365.
22 Y. Q. Gao, H. B. Li, G. W. Yang, J. Appl. Phys. 2016, **119**, 034902.

23 N. H. Chou, P. N. Ross, A. T. Bell, T. D. Tilley, *ChemSusChem* 2011, **4**, 1566-1569.
24 B. S. Yeo, A. T. Bell, J. Am. Chem. Soc. 2011, 133, 5587-5593.
[25] M. E. G. Lyons, M. P. Brandon, J. of Electroanal. Chem. 2010, **641**, 119-130
26 R. Matheu, M. Z. Ertem, J. Benet-Buchholz, E. Coronado, V. S. Batista, X. Sala, A. Llobet, *J. Am. Chem. Soc.* 2015, **137**, 10786-10795.